Acta Biochim Biophys Sin 2023, 55(12): 1938–1949
https://doi.org/10.3724/abbs.2023241
Advance Access Publication Date: 15 November 2023
Original Article

Original Article

Mesenchymal stem cell exosomes inhibit nucleus pulposus cell apoptosis via the miR-125b-5p/TRAF6/NF-κB pathway axis

Yang Duan[1,†], Cheng Yu[1,†], Wenhao Kuang[1], Jianjun Li[1], Sujun Qiu[1], Songjia Ni[2], and Zhong Chen[1,*]

[1]Department of Spinal Surgery, Zhujiang Hospital, Southern Medical University, Guangzhou 510260, China, and [2]Department of Orthopedics and Traumatology, Zhujiang Hospital, Southern Medical University, Guangzhou 510260, China
[†]These authors contributed equally to this work.
*Correspondence address. Tel: +86-20-61643888; E-mail: chenzhong@smu.edu.cn

Received 17 January 2023 Accepted 7 July 2023

Abstract

Intervertebral disc degeneration (IVDD) is the pathological basis of a range of degenerative spinal diseases and is the primary cause of lower back pain. Mesenchymal stem cell (MSC) transplantation inhibits IVDD progression. However, the specific mechanisms that underlie these effects remain unclear. In this study, candidate microRNAs (miRNAs) are screened using bioinformatics and high-throughput sequencing. TNF-α is used to induce nucleus pulposus cell (NPC) degeneration. MSC-derived exosomes (MSC-exosomes) are obtained using high-speed centrifugation and identified by transmission electron microscopy (TEM), nanoparticle tracking analysis (NTA) and western blot analysis. Cell viability is determined by CCK-8 assay. Flow cytometry and TUNEL assays are used to detect cell apoptosis. The expression levels of miR-125b-5p are detected by RT-qPCR, and a dual-luciferase gene reporter assay confirms the downstream target genes of miR-125b-5p. Protein expression is determined by western blot analysis. Rat models are used to validate the function of miR-125b-5p in MSC-exosomes. The results show that miR-125b-5p is expressed at low levels in degenerated disc tissues compared with that in normal disc tissues; however, it is highly expressed in MSC-exosomes. Furthermore, MSC-exosomes are efficiently taken up by NPCs while miR-125b-5p is delivered into NPCs; thus, MSC-exosomes act as inhibitors of apoptosis in NPCs. Overexpression of miR-125b-5p downregulates TRAF6 expression and inhibits NF-κB activation. However, TRAF6 overexpression reverses these effects of miR-125b-5p. We demonstrate that MSC-exosomes attenuate IVDD *in vivo* by delivering miR-125b-5p. MSC-exosomes can deliver miR-125b-5p to target TRAF6, inhibit NF-κB activation, and attenuate the progression of IVDD.

Key words exosome, miR-125b-5p, TRAF6, NF-κB, apoptosis

Introduction

Intervertebral disc degeneration (IVDD) is the pathological basis of degenerative spinal disorders that can lead to intractable back pain [1]. Recently, IVDD has been characterized by a decrease in the extracellular matrix (ECM), inflammatory response, and nucleus pulposus cell (NPC) senescence [2,3]. NPCs promote the production of the extracellular matrix to maintain the hydrated state of the nucleus pulposus, the inner core of the vertebral disc. Noticeably, dehydration of the nucleus pulposus triggers the loss of disc height and deformation, segmental instability, and pain induction [4]. Current clinical treatments for IVDD include nonpharmacological treatments such as exercise, weight loss, and physical therapy, as well as pharmacological treatments such as nonsteroidal anti-inflammatory drugs, hormones, opioid analgesics, and surgery [5,6]. However, these treatment approaches all aim at relieving pain or compressing the nerve roots or spinal cord by intervertebral discs to alleviate symptoms, but they do not prevent or reverse the pathological process of IVDD [5,7]. Furthermore, the mechanism of

© The Author(s) 2023. This is an open access article distributed under the terms of the Creative Commons Attribution-NonCommercial-NoDerivs License (https://creativecommons.org/licenses/by-nc-nd/4.0/).

IVDD is not completely understood. Therefore, it is of great clinical importance to further investigate the pathogenesis of IVDD and explore novel treatment therapies.

Exosomes are nanoscale extracellular vesicles composed of lipid bilayers, and their diameter ranges from 50–200 nm with an average diameter of 100 nm [8]. Exosomes originate when, in the endocytic pathway, the cell membrane buds inwards to form early secretory endosomes and intracellular multivesicular bodies (MVBs) containing intraluminal vesicles (ILVs). Subsequently, ILVs are secreted into exosomes when they fuse with the plasma membrane [7,9]. Recent research indicates that exosomes regulate intercellular communication by delivering a variety of bioactive molecules (mRNAs, miRNAs, and proteins) and lipids [10,11]. Importantly, the ability of exosomes to deliver miRNAs to target cells has been recently shown to have therapeutic effects [12,13]. It has been reported that intradiscal transplantation of synovial mesenchymal stem cells prevents intervertebral disc degeneration in rabbits [14]. A growing number of studies have shown that exosomes are an effective treatment for disc degeneration [15]. However, the mechanism of MSC-exosomes on NPCs is not fully clarified.

MicroRNAs (miRNAs) are small noncoding RNAs that regulate gene expression at the posttranscriptional level and induce target mRNA degradation or translational repression [16]. miRNAs regulate various aspects of cellular functions, including growth, proliferation, differentiation, development, metabolism, infection, immunity, cell death, organelle biogenesis, messenger signaling, DNA repair, and self-renewal [17,18]. Recent studies have shown that miRNAs can target mRNAs to regulate the apoptosis of NPCs, the inflammatory response, and collagen synthesis, thereby preventing the progression of IVDD [19–21]. Recent studies have shown that miR-125b-5p can prevent disease progression through the regulation of downstream targets. Cao *et al.* [22] demonstrated that miR-125b-5p can promote renal injury repair by regulating p53. Rasheed *et al.* [23] demonstrated that miR-125b-5p can alleviate paracetamol-induced acute liver injury. Therefore, unravelling the effects of miR-125b-5p on its potential target mRNAs is essential for gaining an understanding of the molecular mechanisms of IVDD and identifying new therapeutic targets for IVDD.

Tumor necrosis factor receptor (TNFR)-associated factor 6 (TRAF6) is a family of linker proteins involved in signaling through members of the TNF receptor family and Toll/interleukin-1 receptor (TIR) family. TRAF molecules regulate the activation of the IKK complex (IKKα and IKKβ), leading to the activation of the NF-κB signaling pathway [24]. Previous studies have demonstrated that TRAF6 regulates the inflammatory response by modulating NF-κB, thereby preventing osteoarthritis [23]. However, the regulatory relationship between miR-125b-5p and TRAF6 in intervertebral discs has not yet been clarified.

In this study, we identified that miR-125b-5p is strongly associated with IVDD and is a crucial molecule for the therapeutic effect of MSC-exosomes. We believe that our findings provide a novel perspective on MSC-exosomes for the treatment of IVDD and are potentially valuable for the development of novel treatment strategies for IVDD.

Materials and Methods

Cell culture

Human NPCs were purchased from ScienCell (San Diego, USA) and were cultured in Dulbecco's modified Eagle's medium (DMEM; Gibco, New York, USA) containing 10% fetal bovine serum (FBS; Invitrogen, Carlsbad, USA) and 1% penicillin-streptomycin in T25 flasks at 37°C and 5% CO_2. When the NPCs grew to 90% confluence, they were digested with 0.25% trypsin/1 mM EDTA and then transferred to larger flasks for expansion. The third- and fourth-generation NPCs were used for subsequent experiments.

Bone marrow mesenchymal stem cells (BMSCs) were purchased from Procell (Wuhan, China). BMSCs were cultured in low-sugar medium (α-MEM; Gibco) containing 10% FBS and 1% penicillin-streptomycin. MSCs from the third and fourth generations were used for subsequent experiments.

Exosome isolation

MSC-exosomes were extracted using Exosome Concentration Solution (ECS; Umibio, Shanghai, China) according to the manufacturer's instructions. Briefly, when the MSCs grew to a density of 50%–60%, the medium was changed to a medium containing 10% FBS without exosomes, and after 48 h of culture, the supernatant was collected and stored at –80°C. When a sufficient amount of supernatant was collected, it was thawed at 4°C, transferred to a centrifuge tube at 4°C and centrifuged at 3000 *g* for 10 min to remove the cell debris. The supernatant was transferred to a new centrifuge tube, and ECS was added at a ratio of 5:1. After addition of the ECS reagent, the supernatant mixture was mixed with a vortex shaker for 1 min and then kept for 2 h at 2–8°C. Subsequently, the mixture was centrifuged at 10,000 *g* at 4°C for 60 min, and the supernatant was discarded. The remaining pellet was rich in exosomal particles. Next, the exosomes were resuspended in 100 μL of PBS, transferred to another 1.5 mL centrifuge tube and stored at –80°C for subsequent experiments.

Exosome characterization

Exosome particle size and concentration were measured by nanoparticle tracking analysis (NTA) at Viva Cell Bioscience (Shanghai, China) with Zeta View PMX 110 (Particle Metrix, Meerbusch, Germany) and the corresponding software Zeta View 8.04.02. Isolated exosome samples were appropriately diluted with PBS to measure the particle size and concentration. NTA measurements were recorded and analyzed at 11 positions. The Zeta View system was calibrated using 110 nm polystyrene particles.

The brief procedure of the transmission electron microscopy (TEM) assay was as follows. The exosomes were resuspended in 100 μL of 2% PFA, and 5 μL of exosome suspension was added to the Formvar-carbon-loaded copper mesh; the mesh (Formvar side down) was placed on a PBS droplet and washed, the Formvar side was kept moist, and the other side was kept dry during all steps. The copper mesh was placed on a 50 μL 1% glutaraldehyde drop for 5 min; the mesh was placed on 100 μL ddH_2O for 2 min (repeated eight times); the mesh was placed on a 50-μL UO2 oxalate drop for 75 min and a 50-μL methylcellulose drop for 10 min; excess liquid was blotted off on a filter paper; the mesh was air dried for 10 min; and electron micrographs were taken at 80 kV with a transmission electron microscope (JEOL, Tokyo, Japan).

The expressions of exosome marker proteins (CD63, CD81, TSG101 and calnexin) were detected by western blot analysis.

Exosome sequencing and bioinformatics analysis

RNA from the MSC-exosomes was extracted using the TRIzol kit (TaKaRa, Otsu, Japan) according to the manufacturer's protocol,

and the concentration and purity of RNA were assayed using a NanoDrop 2000 spectrophotometer (Thermo Fisher Scientific, Waltham, USA). Each purified RNA sample was used for reverse transcription, PCR amplification, and miRNA library construction. Sequencing was performed in SE75 mode using the NextSeq CN500 sequencing platform (Illumina, San Diego, USA). The raw sequencing data were also evaluated by FAST-QC, including the quality distribution of nucleotides, position-specific sequencing quality, GC content, proportion of PCR duplication, and kmer frequency. The mapping of small RNA was performed using an internationally recognized BWA algorithm [25]. The clean reads were compared with the miRNA database of the corresponding species to obtain miRNA expression.

According to the GEO dataset GSE116726 (including three nucleus pulposus samples from traumatic lumbar fracture patients and three nucleus pulposus samples from intervertebral disc degeneration patients) expression matrix data, the data were analyzed using the limma function in R language to screen differentially downregulated miRNAs in the analysis results of differential expression. Based on the exosome sequencing data, we screened the exosome sequencing data for miRNAs with high expression in the MSC-exosome group and low expression in the IVDD group.

To predict the targets of miR-125b-5p, online databases, including microT-CDS (http://diana.imis.athena-innovation.gr/DianaTools/index.php?r=microT_CDS/index), TargetScan (http://www.targetscan.org/), and miRDB (http://mirdb.org/), were used.

Exosome uptake by NPCs

Exosome uptake was measured using PKH26 (Umibio) according to the manufacturer's instructions. Briefly, the purified MSC-exosomes were incubated with PKH26 for 5 min at room temperature, and then the labelled exosomes were washed 2–3 times with PBS, followed by centrifugation at 120,000 *g* for 90 min and resuspension in the culture medium. After suspension, the NPCs were incubated at 37°C for 12 h. The NPCs were washed twice with PBS. The nuclei were stained with Hoechst33342 (Solarbio, Beijing, China) for 10 min and finally observed under a fluorescence microscope (Leica, Wetzlar, Germany). In the follow-up experiments, NPCs were incubated with 20 μg of exosomes.

RNA extraction and real-time quantitative PCR

Total RNA was isolated from human NPCs using the TRIzol kit according to the manufacturer's instructions. Reverse transcription was performed using 1000 ng of total RNA and a PrimeScript RT Reagent Kit (TaKaRa) or a PrimeScript RT Master Mix (TaKaRa) to study miRNA and mRNA expression, respectively. For miRNA assays, the reverse reaction was performed at 42°C for 15 min, followed by inactivation at 85°C for 5 s. qRT-PCR amplification was performed using the CFX Connection Real-Time System (Bio-Rad, Hercules, USA) and the SYBR Premix Ex Taq II kit (TaKaRa). The following cycling conditions were used: 95°C for 30 s, followed by 40 cycles of 95°C for 5 s and 60°C for 30 s. All reactions were duplicated with miRNA normalized to the internal reference *U6* and mRNA normalized to *GAPDH*. The $2^{-\Delta\Delta CT}$ method was used to assess relative mRNA and miRNA expression levels. The primer sequences are shown in Table 1.

Cell counting kit-8 assay

The proliferation capacity of the NPCs was determined using the Cell Counting Kit 8 (CCK-8; APExBIO, Houston, USA). NPCs were seeded in 96-well plates at a density of 8×10^3 cells/well. Each well was supplemented with 200 μL of complete medium. Next, 10 μL CCK-8 reagent/well was added after 0, 24, 48, and 72 h and incubated at 37°C for 1 h sheltered from light. Then, the optical density (OD) was measured at 450 nM using an ELX808 microplate reader (Bio-Tek, Vermont, USA). Each assay was performed in triplicate.

NPC degeneration model

The NPCs were inoculated in 96-well plates at 5000 cells per well, supplemented with 200 μL of complete medium, and placed in a cell culture incubator at 37°C with 5% CO_2 overnight. Then, the medium was discarded from each well, the plates were washed gently twice with PBS and complete medium containing TNF-α (100 ng/mL; Peprotech, New Jersey, USA) was added. Finally, NPC activity was detected using the CCK-8 method at 0, 24, 48, and 72 h.

TUNEL analysis

NPCs were seeded onto 15-mm cell slides in 24-well plates. PFA (4%) was first used to fix cells for 15 min, and 0.5% Triton X-100 was applied for 20 min to permeate cells. The plates were washed 3 times (5 min each) with PBS; then, 50 μL TUNEL reaction solution (45 μL fluorescent labelling solution with 5 μL TdT enzyme mixed in dark) was added, and the plates were incubated for 60 min at 37°C in darkness. The plates were subsequently washed with PBS, 100 μL Hoechst33342 staining solution was added, and the plates were incubated for 5 min at 37°C without light. Subsequently, the

Table 1. The sequences of primers used in this study

Gene	Forward primer (5′→3′)	Reverse primer (5′→3′)
miR-125b-5p	CGCGTCCCTGAGACCCTAAC	AGTGCAGGGTCCGAGGTATT
U6	CGCTTCGGCAGCACATATAC	TTCACGAATTTGCGTGTCAT
Bax	CGAACTGGACAGTAACATGGAG	CAGTTTGCTGGCAAAGTAGAAA
Bcl-2	GACTTCGCCGAGATGTCCAG	GAACTCAAAGAAGGCCACAATC
Caspase-3	CCAAAGATCATACATGGAAGCG	CTGAATGTTTCCCTGAGGTTTG
TRAF6	GAGACAGGTTTCTTGTGACAAC	TGGCAACCAAAAGTACTGAATG
GAPDH	GCACCGTCAAGGCTGAGAAC	TGGTGAAGACGCCAGTGGA
rno-miR-125b-5p	AAGCTGAGTCCCTGAGACCCTAA	ATCCAGTGCAGGGTCCGAGG
Traf6	AATCACTTGGCACGGCACTTG	GGAGAGGAGGCATCGCATGG

Hoechst33342 staining solution was removed, and the plates were washed with PBS. Next, 10 μL of anti-fluorescence quencher was added, then the slides were carefully removed from the wells and fluorescence images were obtained using the fluorescence microscope.

Apoptosis assay

The apoptosis ratio of NPCs was determined using an apoptosis kit (Solarbio) according to the manufacturer's instructions. The cell culture medium was carefully collected, EDTA-free trypsin (Solarbio) was added, and afterwards, the previously collected medium was added to terminate the digestion. The cells were gently resuspended and transferred into a centrifuge tube before centrifugation at 300 *g* at 4°C for 5 min. Next, the supernatant was discarded, and binding buffer (Solarbio) was added to adjust the cell concentration to 5×10^6 cells/mL. Then, 100 μL of the cell suspension was added to a 5-mL flow tube, along with 5 μL Annexin V/FITC (Solarbio) and incubated in the dark at room temperature for 5 min. Finally, 5 μL of propidium iodide solution (PI; Solarbio) and 400 μL PBS were added to the flow tube, and cells were immediately analyzed by flow cytometry (cytoFLEX; Beckman, California, USA).

Western blot analysis

Radioimmunoprecipitation analysis (RIPA) lysis buffer (Solarbio) was used to extract proteins from NPCs and rat intervertebral discs, and BCA protein assay kits (Cowin, Beijing, China) were used to quantify proteins. Proteins were separated by 10% SDS-PAGE and then transferred to polyvinylidene fluoride membranes (Millipore, Billerica, USA), blocked for 30 min using Rapid Blocking Solution (Beyotime, Beijing, China), and incubated with the appropriate primary antibodies overnight at 4°C. The membranes were then washed three times with TBST and subsequently incubated with the corresponding HRP-conjugated secondary antibody at room temperature for 2 h. Afterwards, the membranes were washed again for three times with TBST. After washing, the chemiluminescence intensity of the blots was detected using ECL (Millipore) and a chemiluminescence system (Bio-Rad). The following antibodies were used: GAPDH (1:5000 dilution; Proteintech, Rosemont, USA), CD63/CD81/TSG101/calnexin (1:1000 dilution; Abcam, Cambridge, USA), Bax, Bcl-2, Caspase-3, TRAF6, IκBα, p-IκBα, p65, and p-p65 (1:1000 dilution; Proteintech), and HRP-conjugated goat anti-mouse/rabbit secondary antibody (1:5000 dilution; Proteintech).

Cell transfection assay

NPCs were seeded in 6-well plates at a density of 3×10^5 cells/well and reached approximately 70% confluence after 48 h. The plates were then treated with 100 nM miR-125b-5p mimic (5′-UCCCUGAGACCCUAACUUGUGA-3′), miR-NC (5′-UUCUCCGAACGUGUCACGUTT-3′), miR-125b-5p inhibitor (5′-UCACAAGUUAGGGUCUCAGGGA-3′), or inhibitor NC (5′-CAGUACUUUUGUGUAGUACAA-3′) (GenPharma, Shanghai, China) using Lipofectamine 2000 (Life Technologies Corporation, Carlsbad, USA) at a concentration of 30 nM according to the manufacturer's instructions. For plasmid transfection, 3 μg NC plasmid or TRAF6 plasmid (GenPharma) was transfected into NPCs using 5 μL of Lipofectamine 2000. After transfection for 48 and 72 h, the cells were collected for RT-PCR and western blot analysis.

Dual luciferase reporter gene assay

HEK239 cells (Hycyte, Soochow, China) were seeded in 6-well plates at 3.5×10^5 cells/well. Next, 500 ng TRAF6 wild-type plasmid or TRAF6 mutant plasmid, 50 nmol miR-125b-5p mimics, or miR-125b-5p NC were cotransfected using Lipofectamine 2000. After 6 h, the medium was replaced by complete medium, and the cells were lysed for fluorescence detection after 48 h. The firefly luciferase reaction and Renilla luciferase working solutions (GenePharma) were prepared according to the protocol. The cell lysate (20 μL) was added to a black enzyme-labelled plate. Firefly luciferase working solution (100 μL) and *Renilla* luciferase working solution were added and incubated for 10 min, and then the luciferase activity was detected.

Animal experiments

Surgical procedures were performed on adult (aged 10 weeks) male Sprague-Dawley (SD) rats (Guangdong Medical Laboratory Animal Center, Guangzhou, China) weighing 200–250 g. All rats were housed in a standard animal room at a 12:12 h light:dark cycle with free access to food and water. Twenty rats were randomly assigned into sham-operated, IVDD, IVDD + exo, and IVDD + exo$^{\text{anti-miR-125b-5p}}$ groups. The rats were anaesthetized with 1.5% isoflurane, the abdominal hair of the rats was shaved out with a skin preparation cutter, and after disinfection with iodophor, an incision of approximately 5 cm was made in the left abdomen using a scalpel. The peritoneum and abdominal organs were carefully drawn to the right to expose the gap between the posterior peritoneum and the left psoas major muscle. Then, the posterior peritoneum and abdominal organs were drawn to the right to locate the L4/5 intervertebral disc, and a puncture injury was performed using a straight-tipped microscalpel. The disc was pierced vertically in the middle to a depth of approximately 2 mm; then, using a curved-tip microscalpel, some of the nucleus pulposus tissue was destroyed and removed [26]. Subsequently, 0–4 absorbable sutures were used to close the incision. The procedure in the sham-operated group was similar to that in the IVDD group, but the tip of the knife only touched the surface of the disc without penetrating it. One week after surgery, 2 μL of sterile saline containing exosomes (approximately 1.5×10^6 particles) was injected into the injured disc, and the injection was repeated once after 2 weeks. At the end of the fourth week postsurgery, the rats were subjected to magnetic resonance imaging (MRI) examination and then sacrificed, and segmental discs were removed for subsequent analyses. All experiments and surgical procedures were approved by the Animal Ethics Committee of the Zhujiang Hospital of Southern Medical University (LAEC-2020-203).

Magnetic resonance imaging (MRI) and histological analysis

MRI was performed on all rats using a 7.0 T animal-specific MRI system (Bruker PharmaScan, Lucken, Germany). The degree of disc degeneration was assessed according to the Pfirrmann classification (Supplementary Table S1) [27,28]. After MRI, the rats were euthanized, and the corresponding segmental discs were taken for histological examination. For Safranin O-Fast Green (SOFG) staining, each paraffin-embedded sample was sectioned at 4 μm and stained with 0.2% Safranin O solution (Sigma-Aldrich, St Louis, USA) for 15 min and with 0.2% Fast Green solution (Sigma-Aldrich) for 5 min. For HE staining, hematoxylin staining solution (Sigma-

Aldrich) was added to the sections and incubated for 5 min. Sections were rinsed to remove excess staining solution, and then eosin staining solution (Sigma-Aldrich) was added to the sections and incubated for 2 min. Then, sections were dehydrated in ethanol and incubated with xylene for 5 min. Finally, the slices were sealed with neutral gum and subject to microscopic observation.

Immunofluorescence analysis

For immunofluorescence (IF) analysis, sections were prepared using the same method of SOFG staining. After dewaxing, the sections were repaired with improved citrate antigen retrieval solution (Beyotime) in a boiling water bath for 30 minutes. Then, 0.5% Triton (Beyotime) was used to permeate the cell membrane for 20 min, and immunol staining blocking buffer (Beyotime) was used for blocking for 1 h. Then, the sections were incubated with the primary antibody (TRAF6 or p-p65, 1:100 dilution) overnight at 4°C, followed by incubation with anti-rabbit Alexa Fluor 488 secondary antibody (1:500 dilution; APExBIO) at 37°C for 1 h. Finally, the nuclei were stained with DAPI. IF images were obtained under the fluorescence microscope and analyzed using ImageJ software (NIH, Bethesda, USA).

Statistical analysis

All experiments were repeated three or more times. Data are expressed as the mean ± standard deviation (SD). GraphPad Prism 8.0 software (GraphPad, La Jolla, USA) was used. Independent samples *t*-test analysis was used to compare whether the means were significantly different between the two groups. One-way ANOVA was used when multiple samples were compared. Data were considered statistically significant when $P < 0.05$.

Results

The expression of miR-125b-5p is reduced in degenerated discs and TNF-α-induced NPCs but is highly expressed in MSC-exosomes

To detect the expression of miR-125b-5p in IVDD, we screened 152 differentially expressed miRNAs with adjusted $P < 0.01$ and $|\log FC| > 2$ as the threshold. Among the screened miRNAs, 59 miRNAs were upregulated and 93 miRNAs were downregulated (Figure 1A). Based on the MSC-exosome sequencing data, we further screened the miRNAs that had high expression levels in MSC-exosomes and were downregulated in IVDD (Figure 1B,C). The top five miRNAs were hsa-let-7b-5p, hsa-let-7i-5p, hsa-miR-125b-5p, hsa-let-7a-5p, and hsa-miR-221-3p. Next, we detected the expression of miR-125b-5p in TNF-α-induced NPCs. Consistently, the expression of miR-125b-5p gradually decreased with increasing TNF-α stimulation (Figure 1D).

Identification of MSC-exosomes and uptake by NPCs

We identified exosomes by TEM, NAT, and western blot analysis,

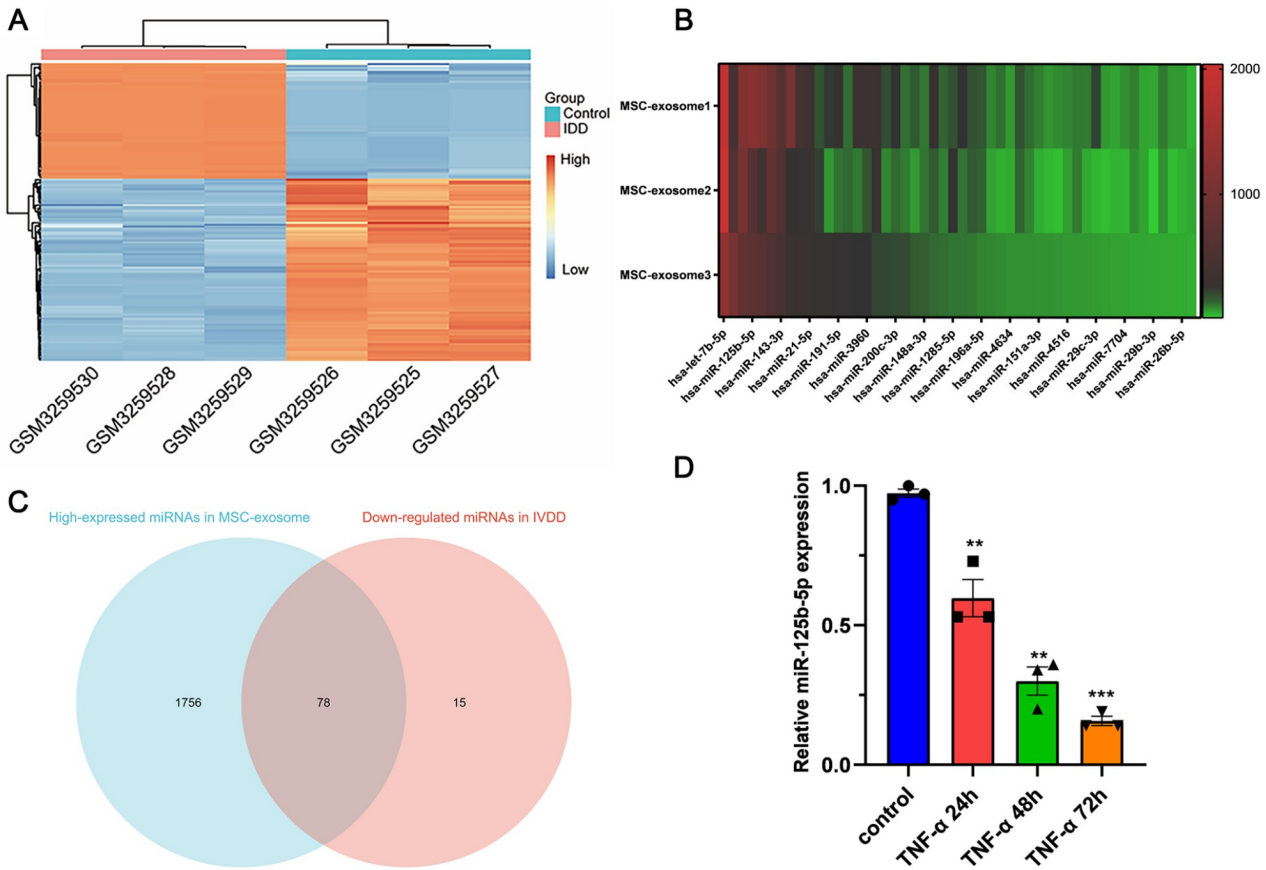


Figure 1. miR-125b-5p is strongly associated with the development of IVDD (A) Expression of miRNAs in GSE116726 dataset. (B) Heat map of exosome sequencing results. $n = 3$. (C) Exosome sequencing results are intersected with the GSE116726 dataset. (D) With the extension of TNF-α stimulation time, miR-125b-5p expression gradually decreased. $n = 3$. $^*P < 0.05$, $^{**}P < 0.01$, $^{***}P < 0.001$. Student's *t*-test was used for comparison between two groups.

and the extracted exosomes showed nanoscale vesicles with a bilayer structure under TEM (Figure 2A). The average diameter and concentration of the extracted exosomes via NAT were 128.8 nm and 2.2×10^6 particles/mL, respectively (Figure 2B). Western blot analysis results showed that exosomes we extracted and positive controls expressed the marker proteins TSG101, CD63 and CD81, but did not express Calnexin (Figure 2C). PKH26-labelled exosomes showed red fluorescence, and the nuclei of Hoechst33342-labelled NPCs showed blue fluorescence. To demonstrate that exosomes could be taken up by NPCs, we cocultured PKH26-labelled exosomes with Hoechst33342-labelled NPCs and observed clear red fluorescence in the cytoplasm of NPCs by fluorescence microscopy, which indicated that NPCs took up exosomes (Figure 2D).

MSC-exosomes inhibit TNF-α-induced NPC apoptosis by delivering miR-125b-5p

To determine the most suitable TNF-α concentration for the cell model, we detected NPC cell activity at different concentrations and time intervals by CCK-8 assay. The results indicated that NPC activity was decreased with increasing stimulation time and concentration, and when induced with 100 ng/mL TNF-α for 48 h, NPC activity was decreased to 68.6% (Figure 3A). This concentration was selected for the cell degeneration model. Subsequently, we cocultured exosomes and MSC-exosomes transfected with miR-125b-5p inhibitor (exoanti-miR-125b-5p) with NPCs and detected the expression of miR-125b-5p in NPCs by RT-qPCR. The results revealed a 21.9-fold increase in miR-125b-5p expression in the exosome group compared to that in the control group. Additionally, the expression of miR-125b-5p in the exoanti-miR-125b-5p group was not significantly different from that in the control group (Figure 3B). Therefore, transfection with miR-125b-5p inhibitor specifically downregulated miR-125b-5p expression in MSC-exosomes. Exosomes can inhibit the suppressive effect of TNF-α on NPC proliferation as revealed by the CCK-8 assay (Figure 3C), indicating the protective effect of MSC-exosomes. However, this protective effect disappeared when *miR-125b-5p* was knocked down, suggesting that this protective effect is strongly associated with miR-125b-5p in exosomes. Flow cytometry and TUNEL staining showed that the apoptosis rate of NPCs after exosome uptake was significantly lower than that of NPCs after exoanti-miR-125b-5p uptake under TNF-α stimulation. This suggests that exosomes have an anti-apoptotic effect on NPCs, which is lost after specific knockdown of *miR-125b-5p*. The percentage of TNF-α-induced apoptotic NPCs was reduced by exosomes but not by exoanti-miR-125b-5p (Figure 3D–G). Next, we observed the growth of NPCs induced by TNF-α using an inverted microscope. The cell density and morphology of NPCs after exosome uptake were not significantly different from those of the control group, whereas NPCs after uptake of exoanti-miR-125b-5p showed lower cell density (Figure 3H,I). In addition, the expressions of Bax and cleaved caspase-3 were significantly decreased in NPCs that took up exosomes compared to those that took up exoanti-miR-125b-5p. Consistently, the expression of Bcl-2 was increased in NPCs treated with exosomes (Figure 3J–L). These results suggest that miR-125b-5p in exosomes plays a role in promoting NPC proliferation and inhibiting apoptosis.

miR-125b-5p inhibits NF-κB signaling pathway activation by directly targeting TRAF6

To explore the potential target genes of miR-125b-5p related to the NF-κB signaling pathway, we intersected the TargetScan, microTCDS, miRDB and NF-κB core genes. The results indicated that *TRAF6* may be a potential target gene of miR-125b-5p (Figure 4A). Next, we detected miR-125b-5p expression by RT-qPCR. The results showed a 216.5-fold increase in miR-125b-5p expression in NPCs

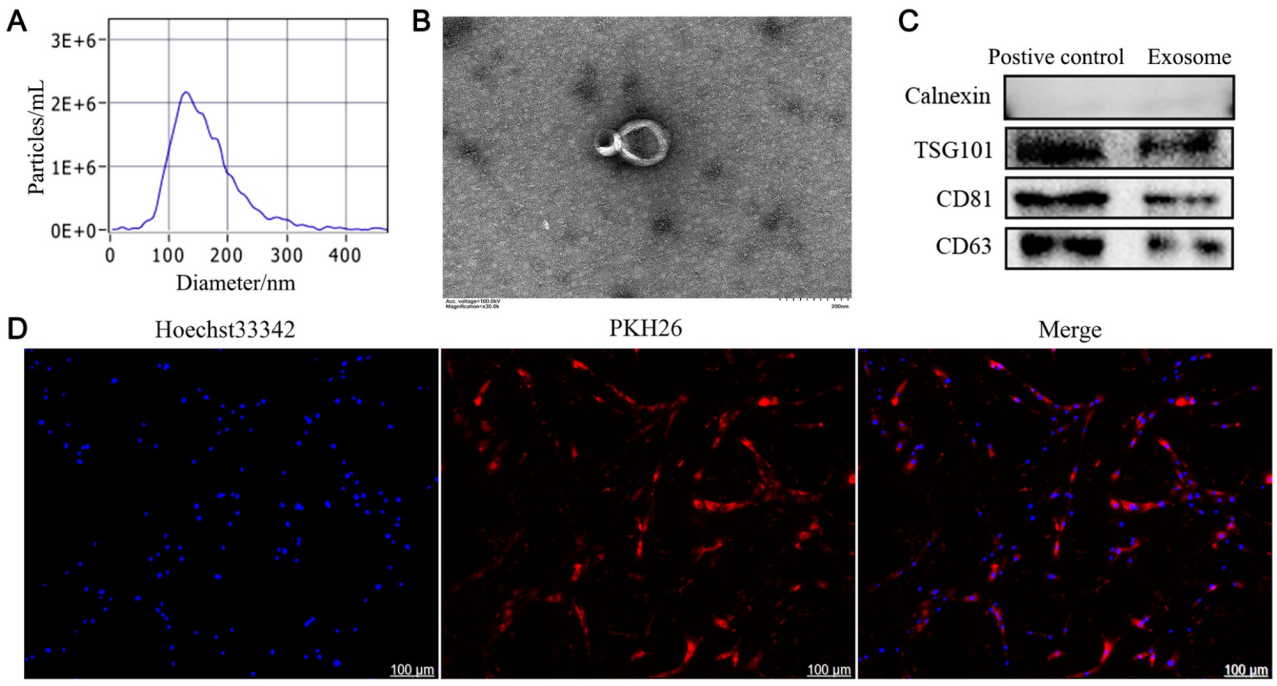


Figure 2. Identification of exosomes and efficient uptake of exosomes by NPCs (A) Nanoparticle tracking analysis. (B) Transmission electron microscopy. Scale bar: 200 nm. (C) Western blot analysis of exosome marker proteins CD63, CD81, TSG101 and Calnexin. (D) Fluorescence microscopy observation exosomes uptake by NPCs. Scale bar: 100 μm.

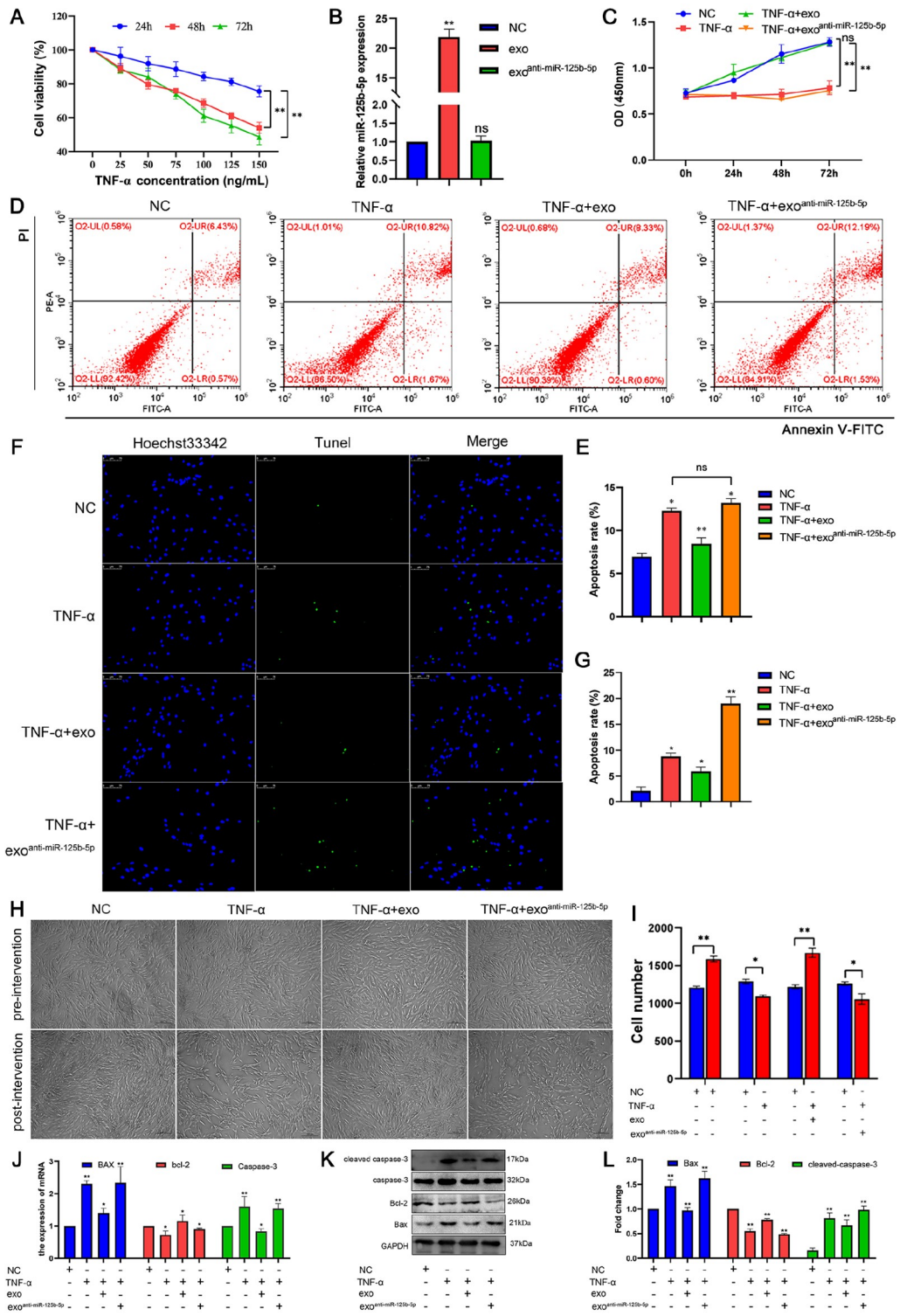


Figure 3. MSC-exosomes deliver miR-125b-5p to inhibit TNF-α-induced NPC apoptosis (A) NPC activity gradually decreases with increasing TNF-α concentration and time. $n=3$. (B) RT-qPCR detection of miR-125b-5p expression in NPCs after taking up exosome and exoanti-miR-125b-5p. $n=3$. (C) Optical density of NPCs uptaking exosome and exoanti-miR-125b-5p under TNF-α stimulation. $n=3$. (D,E) Apoptosis of NPCs uptaking exosome and exoanti-miR-125b-5p under TNF-α stimulation analyzed by flow cytometric assay. $n=3$. (F,G) TUNEL assay for apoptosis in NPCs uptaking exosome and exoanti-miR-125b-5p under TNF-α stimulation. Scale bar: 75 μm. $n=3$. (H, I) Cell density and morphology of NPCs uptaking exosome and exoanti-miR-125b-5p under TNF-α stimulation. Scale bar: 200 μm. $n=3$. (J) RT-qPCR detection of caspase 3, bax and bcl mRNA in NPCs uptaking exosomes and exoanti-miR-125b-5p under TNF-α stimulation. $n=3$. (K,L) Western blot analysis of cleaved caspase 3, caspase 3, bax and bcl expressions in NPCs uptaking exosomes and exoanti-miR-125b-5p under TNF-α stimulation. $n=3$. ns: no significant difference. $^*P<0.05$, $^{**}P<0.01$. Student's *t*-test and one-way ANOVA were used for comparison between two groups and multiple groups, respectively.

transfected with miR-125b-5p mimics compared to the control, whereas miR-125b-5p expression in NPCs transfected with miR-125b-5p inhibitors decreased by 28.5% (Figure 4B). This result suggests that miR-125b-5p mimics or inhibitors can effectively increase or decrease the expression of miR-125b-5p. Additionally, we detected the expression of TRAF6 in NPCs after transfection with miR-125b-5p mimics or inhibitors, and the results showed that the expression of TRAF6 was significantly decreased after overexpression of miR-125b-5p. In contrast, the expression of TRAF6 was significantly increased following a reduction in the expression of miR-125b-5p (Figure 4C,D). To confirm the direct binding of miR-125b-5p to the 3′-UTR of TRAF6 mRNA, we performed luciferase activity assays. miR-125b-5p mimics markedly suppressed the luciferase activity of cells transfected with the wild-type 3′-UTR of *TRAF6* but not in cells transfected with the mutant 3′-UTR of *TRAF6* (Figure 4E). To detect the activation of the NF-κB signaling pathway, we measured the expression of phosphorylated p65 and IκBα in NPCs transfected with miR-125b-5p mimics or miR-125b-5p mimics and TRAF6 overexpression plasmids. The results showed that miR-125b-5p mimics markedly decreased the expressions of phosphorylated p65 and IκBα in NPCs. However, overexpression of TRAF6 reversed the inhibitory effect of miR-125b-5p on NF-κB. The expression levels of p65 and IκBα were not significantly altered following transfection of miR-12b-5p mimics alone or with TRAF6 overexpression plasmids (Figure 4F,G). We observed the proliferation of NPCs after transfection with miR-125b-5p mimics and TRAF6 overexpression plasmids by microscopy. The results showed that overexpression of TRAF6 reversed the proliferative effect of miR-125b-5p (Figure 4H,I). Taken together, the above results demonstrate that miR-125b-5p directly targets *TRAF6* and inhibits NF-κB signaling pathway activation.

Injection of exosomes into rat intervertebral discs alleviates IVDD

To confirm the *in vivo* effect of exosomes on IVDD, we used a rat disc degeneration model. We performed MRI in rats and demonstrated that exosomes attenuated disc degeneration, whereas when *miR-125b-5p* was knocked down in exosomes, no such protective

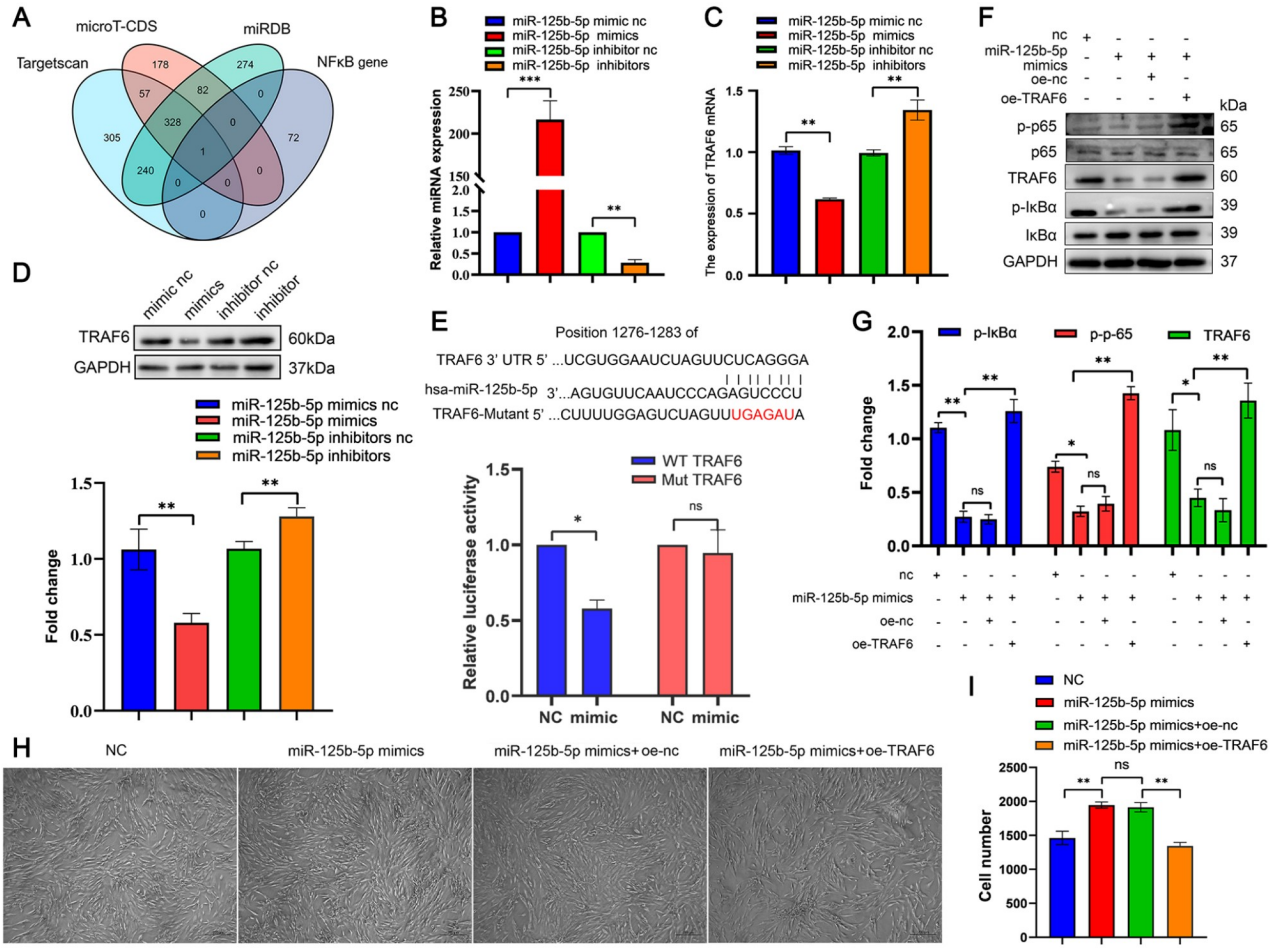


Figure 4. miR-125b-5p targets TRAF6 to inhibit the NF-κB pathway (A) Venn diagram showing the overlap of target genes predicted by Targetscan, miRDB, microT-CDS for miR-125b-5p and NF-κB core genes. (B) RT-qPCR was used to detect miR-125b-5p expression in NPCs after transfection with miR-125b-5p mimics or inhibitors. $n=3$. (C,D) RT-qPCR or western blot analysis were used to detect TRAF6 expression in NPCs after transfection with miR-125b-5p mimics or inhibitors. $n=3$. (E) Luciferase reporter assay revealed that miR-125b-5p exclusively decreased luciferase activity of the wild-type reporter plasmids. $n=3$. (F,G) Western blot analysis of p65, p-p65, IκBα and p-IκBα expressions in NPCs transfected with miR-125b-5p mimics or miR-125b-5p mimics with TRAF6 overexpression plasmids. $n=3$. (H,I) Proliferation of NPCs after transfection with miR-125b-5p mimics and TRAF6 overexpression plasmids. Scale bar: 200 μm. $n=3$. ns: no significant difference. $^*P<0.05$, $^{**}P<0.01$. Student's *t*-test was used for comparison between two groups.

effects were detected (Figure 5A). Discs after exosome injection had lower Pfirrmann scores (Figure 5B). HE staining showed that exosomes could inhibit IVDD progression, and this protective effect was lost after knocking down *miR-125b-5p* in exosomes (Figure 5C). Furthermore, Safranin O and Fast Green staining showed that exosomes prevented the destruction of intervertebral disc cartilage, and this protective effect was lost after the knockdown of *miR-125b-5p* (Figure 5D). Discs had lower histological scores after exosome injection (Figure 5E). RT-qPCR analysis showed that the expression of miR-125b-5p was significantly decreased in degenerated rat intervertebral discs; however, miR-125b-5p expression was significantly increased after exosome treatment. The expression of Traf6 was significantly increased in degenerated rat discs, while the expression of Traf6 was significantly decreased after exosome treatment (Figure 5F). Western blot analysis of the expression of Traf6 was consistent with the RT-PCR results. The expressions of p-IκBα and p-p65 were significantly increased in degenerated rat intervertebral discs; however, the expression of both proteins was significantly decreased after exosome treatment (Figure 5G–H). Immunofluorescence results showed that exosomes significantly reduced the expressions of Traf6 and p-p65 in IVDD models. However, when the IVDD model was treated with exoanti-miR-125b-5p, the expressions of Traf6 and p-p65 were increased significantly (Figure 5I). These results demonstrate that *in vivo* exosomes could deliver miR-125b-5p to NPCs and prevent IVDD progression.

Discussion

In this study, we elucidated the role of MSC-exosomes in the progression of IVDD. We found that MSC-exosomes inhibited IVDD progression via delivery of miR-15b-5p, which targeted TRAF6 and inhibited NF-κB activation. Therefore, this study illustrates that

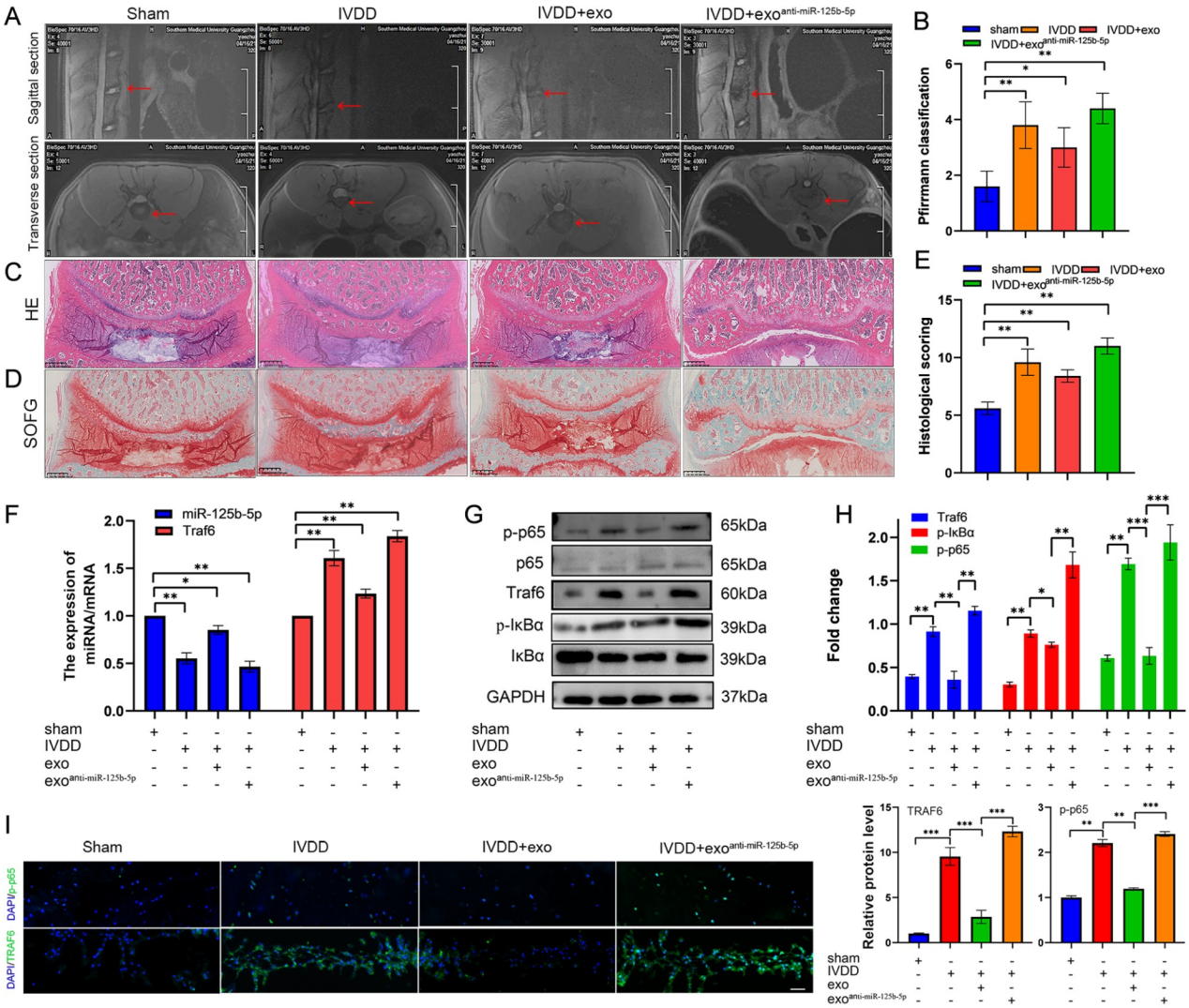


Figure 5. MSC-exosomes deliver miR-125b-5p to alleviate IVDD *in vivo* (A) MRI for *in vivo* experiments. Upper image is sagittal section, and lower image is transverse section. (B) Pfirrmnn score of the intervertebral disc. $n=5$. (C, D) The intervertebral disc is stained with hematoxylin-eosin (HE) and Safranin-O/Fast Green (SOFG). Scale bar: 100 μm. (E) Histological scoring of intervertebral discs. $n=5$. (F) RT-qPCR analysis of miR-125b-5p and Traf6 expression in rat intervertebral discs. $n=5$. (G,H) Western blot analysis of Traf6, IκBα, p-IκBα, p65 and p-p65 expressions in rat intervertebral discs. $n=5$. (I) Immunofluorescence analysis of Traf6 and p-p65 expression in rat intervertebral discs. $n=3$. Scale bar: 50 μm. $^*P<0.05$, $^{**}P<0.01$, $^{***}P<0.001$. Student's *t*-test was used for comparison between two groups.

MSC-exosomes may become part of a novel potential therapeutic strategy for IVDD.

Evidence suggests that miRNAs enriched in cell-secreted vesicles could be potential agents for disease treatment [29]. There is growing evidence that miR-125b-5p exerts various cytoprotective effects. For example, miR-125b-5p attenuates paracetamol-induced stem cell necrosis and thus alleviates acute liver failure [30]. Additionally, Rasheed *et al.* [23] demonstrated that miR-125b-5p moderates the progression of osteoarthritis by regulating the inflammatory response. Furthermore, Yang *et al.* [31] demonstrated that low expression of miR-125b-5p exacerbates the injury induced by lipopolysaccharide (LPS). The role of miR-125b-5p in intervertebral disc degeneration remains unknown. In this study, we found that the expression of miR-125b-5p was downregulated in IVDD and TNF-α-induced degeneration models of NPCs. These results suggest that miR-125b-5p is involved in the regulation of intervertebral disc degeneration.

Multiple studies have confirmed the therapeutic effects of MSC-exosomes by delivering miRNAs. For example, MSC-derived exosomes prevent NPC apoptosis and alleviate disc degeneration by delivering miR-21 [32]. A similar study demonstrated that MSC-derived exosomes, when enriched with miR-142-3p, attenuated NPC apoptosis by targeting MLK3 to inhibit MAPK signaling [13]. Another study reported that BMSC exosomes containing miR-532-5p targeted RASSF5 for delivery of its cargo and inhibited TNF-α-induced apoptosis, ECM degradation, and fibrotic deposition in NPCs [33]. Consistent with these findings, our study showed that NPCs efficiently took up MSC-exosomes, promoted NPC proliferation, and prevented TNF-α-induced apoptosis. Interestingly, these pro-proliferative and anti-apoptotic effects were lost when the expression of miR-125b-5p was specifically downregulated in MSC-exosomes. These results demonstrated that miR-125b-5p is a key molecule for MSC-exosomes to exert this protective effect on NPCs. To the best of our knowledge, this study is the first to investigate the protective effect of exosomal miR-125b-5p against IVDD.

TRAF6 activates IκB kinase, which in turn promotes the downstream nuclear factor (NF)-κB transcription factor and leads to overexpression of proinflammatory cytokine secretion [21]. He *et al.* [34] demonstrated that TRAF6 was inhibited by upregulating miR-146a, thereby attenuating NF-κB p65 activation. Furthermore, Rasheed *et al.* [23] demonstrated that transfection of chondrocytes with a miR-125b mimic significantly inhibited IL-1β-induced transcription of NF-κB p65 and NF-κB p50 and significantly phosphorylated IκBα, confirming the involvement of NF-κB in the regulation of hsa-miR-125b-5p in chondrocytes. Furthermore, Jiang *et al.* [35] demonstrated that in LPS-treated chondrocytes, inhibition of TRAF6 expression significantly reduced the degradation of IκBα and inhibited the transcription of p65. Moreover, knockdown of *TRAF6* by siRNA reduced LPS-induced chondrocyte apoptosis. Zhang *et al.* [36] demonstrated that inhibition of the NF-κB pathway attenuated TNF-α-induced extracellular matrix degradation and senescence of nucleus pulposus cells. It can be concluded that TRAF6 is one of the key factors in activating the NF-κB signaling pathway to promote inflammation and chondrocyte apoptosis. In our study, we found that miR-125b-5p directly targeted TRAF6 to inhibit NF-κB activation. However, cotransfection with the TRAF6 overexpression plasmid reversed the inhibitory effect of miR-125b-5p on the NF-κB pathway, indicating that miR-125b-5p negatively regulates TRAF6 and inhibits NF-κB pathway activation. This is the first demonstration of the involvement of the miR-125b-5p/TRAF6/NF-κB pathway axis in IVDD.

The current treatment options for IVDD include injecting patients with therapeutic proteins and stem cells [37,38]. Furthermore, gene therapy and tissue engineering techniques that involve injection of therapeutic proteins and adenovirus with altered gene expression are reported to undergo significant immune rejection and potential oncogenic risk. Therefore, the treatment option that is currently undergoing clinical trials is stem cell transplantation therapy [39,40]. A few studies showed that injection of hematopoietic stem cells for discogenic back pain did not show any improvement in lower back pain levels after 1 year of follow-up. However, a few other studies came to a different conclusion that injection of MSCs into the intervertebral disc improved pain and MRI performance [41–43]. Disappointingly, there are relatively few relevant clinical trial studies, and the fact that the intervertebral disc is in a state of hypoxia and hypoblood supply is also a great challenge for the survival of transplanted stem cells. Further studies are needed to determine the specific efficacy of stem cell transplantation [7]. Our results suggested that disc injections of MSC-exosomes could significantly inhibit the progression of IVDD; however, the injection of exosome$^{\text{anti-miR-125b-5p}}$ did not significantly inhibit the progression of IVDD. These results suggest that MSC-exosomes inhibit NPC apoptosis by delivering miR-125b-5p. Thus, our study indicates that delivery of miR-125b-5p via MSC-exosomes may be a promising approach for the treatment of IVDD.

Despite the promise of MSC-exosomes in alleviating IVDD, our study had a few limitations. First, we initially screened miR-125b-5p using bioinformatics methods, and a small number of clinical samples were used. Second, we used TNF-α to induce NPC degeneration, which caused a decrease in the expression of miR-125b-5p, the exact mechanism of which deserves further investigation.

In conclusion, this study demonstrates that MSC-exosomes can deliver miR-125b-5p to NPCs to inhibit NPC apoptosis and that this antiapoptotic effect is mediated by miR-125b-5p targeting *TRAF6* to inhibit the NF-κB pathway. Our findings indicate that MSC-exosomes inhibit NPC apoptosis through the miR-125b-5p/TRAF6/NF-κB pathway axis and thereby attenuate IVDD progression.

Funding

This work was supported by the grant from the Zhujiang Hospital of Southern Medical University President's Fund (No. HZQKJJH0399).

Conflict of Interest

The authors declare that they have no conflict of interest.

References

1. Ohnishi T, Iwasaki N, Sudo H. Causes of and molecular targets for the treatment of intervertebral disc degeneration: a review. *Cells* 2022, 11: 394
2. Yang S, Zhang F, Ma J, Ding W. Intervertebral disc ageing and degeneration: the antiapoptotic effect of oestrogen. *Ageing Res Rev* 2020, 57: 100978
3. Liang H, Luo R, Li G, Zhang W, Song Y, Yang C. The proteolysis of ECM in intervertebral disc degeneration. *Int J Mol Sci* 2022, 23: 1715
4. Zhang GZ, Liu MQ, Chen HW, Wu ZL, Gao YC, Ma ZJ, He XG, *et al.* NF-κB signalling pathways in nucleus pulposus cell function and intervertebral

disc degeneration. *Cell Prolif* 2021, 54: e13057
5. Xin J, Wang Y, Zheng Z, Wang S, Na S, Zhang S. Treatment of intervertebral disc degeneration. *Orthopaedic Surg* 2022, 14: 1271–1280
6. Kamali A, Ziadlou R, Lang G, Pfannkuche J, Cui S, Li Z, Richards RG, *et al.* Small molecule-based treatment approaches for intervertebral disc degeneration: current options and future directions. *Theranostics* 2021, 11: 27–47
7. Krut Z, Pelled G, Gazit D, Gazit Z. Stem cells and exosomes: new therapies for intervertebral disc degeneration. *Cells* 2021, 10: 2241
8. Wu P, Zhang B, Shi H, Qian H, Xu W. MSC-exosome: a novel cell-free therapy for cutaneous regeneration. *Cytotherapy* 2018, 20: 291–301
9. Wang C, Guo S, Gu Q, Wang X, Long L, Xiao C, Xie M, *et al.* Exosomes: a promising therapeutic strategy for intervertebral disc degeneration. *Exp Gerontology* 2022, 163: 111806
10. Admyre C, Johansson SM, Qazi KR, Filén JJ, Lahesmaa R, Norman M, Neve EPA, *et al.* Exosomes with immune modulatory features are present in human breast milk. *J Immunol* 2007, 179: 1969–1978
11. Gao M, Gao W, Papadimitriou JM, Zhang C, Gao J, Zheng M. Exosomes—the enigmatic regulators of bone homeostasis. *Bone Res* 2018, 6: 36
12. Zhu LP, Tian T, Wang JY, He JN, Chen T, Pan M, Xu L, *et al.* Hypoxia-elicited mesenchymal stem cell-derived exosomes facilitates cardiac repair through miR-125b-mediated prevention of cell death in myocardial infarction. *Theranostics* 2018, 8: 6163–6177
13. Zhu L, Shi Y, Liu L, Wang H, Shen P, Yang H. Mesenchymal stem cells-derived exosomes ameliorate nucleus pulposus cells apoptosis via delivering miR-142-3p: therapeutic potential for intervertebral disc degenerative diseases. *Cell Cycle* 2020, 19: 1727–1739
14. Miyamoto T, Muneta T, Tabuchi T, Matsumoto K, Saito H, Tsuji K, Sekiya I. Intradiscal transplantation of synovial mesenchymal stem cells prevents intervertebral disc degeneration through suppression of matrix metalloproteinase-related genes in nucleus pulposus cells in rabbits. *Arthritis Res Ther* 2010, 12: R206
15. Hu ZL, Li HY, Chang X, Li YY, Liu CH, Gao XX, Zhai Y, *et al.* Exosomes derived from stem cells as an emerging therapeutic strategy for intervertebral disc degeneration. *World J Stem Cells* 2020, 12: 803–813
16. Conti I, Varano G, Simioni C, Laface I, Milani D, Rimondi E, Neri LM. miRNAs as influencers of Cell–Cell communication in tumor microenvironment. *Cells* 2020, 9: 220
17. Kabekkodu SP, Shukla V, Varghese VK, D'Souza J, Chakrabarty S, Satyamoorthy K. Clustered miRNAs and their role in biological functions and diseases. *Biol Rev* 2018, 93: 1955–1986
18. Yang F, Wang J, Chen Z, Yang Y, Zhang W, Guo S, Yang Q. Role of microRNAs in intervertebral disc degeneration. *Exp Ther Med* 2021, 22: 860
19. Huang Y, Huang L, Li L, Ge Z, Feng G, Liu L, Song Y. MicroRNA-25-3p therapy for intervertebral disc degeneration by targeting the IL-1β/ZIP8/MTF1 signaling pathway with a novel thermo-responsive vector. *Ann Transl Med* 2020, 8: 1500
20. Yun Z, Wang Y, Feng W, Zang J, Zhang D, Gao Y. Overexpression of microRNA-185 alleviates intervertebral disc degeneration through inactivation of the Wnt/β-catenin signaling pathway and downregulation of Galectin-3. *Mol Pain* 2020, 16: 174480692090255
21. Lv F, Huang Y, Lv W, Yang L, Li F, Fan J, Sun J. MicroRNA-146a ameliorates inflammation via TRAF6/NF-κB pathway in intervertebral disc cells. *Med Sci Monit* 2017, 23: 659–664
22. Cao JY, Wang B, Tang TT, Wen Y, Li ZL, Feng ST, Wu M, *et al.* Exosomal miR-125b-5p deriving from mesenchymal stem cells promotes tubular repair by suppression of p53 in ischemic acute kidney injury. *Theranostics* 2021, 11: 5248–5266
23. Rasheed Z, Rasheed N, Abdulmonem WA, Khan MI. MicroRNA-125b-5p regulates IL-1β induced inflammatory genes via targeting TRAF6-mediated MAPKs and NF-κB signaling in human osteoarthritic chondrocytes. *Sci Rep* 2019, 9: 6882
24. Tang X, Zhang L, Wei W. Roles of TRAFs in NF-κB signaling pathways mediated by BAFF. *Immunol Lett* 2018, 196: 113–118
25. Jung Y, Han D. BWA-MEME: BWA-MEM emulated with a machine learning approach. *Bioinformatics* 2022, 38: 2404–2413
26. Qiu S, Shi C, Anbazhagan AN, Das V, Arora V, Kc R, Li X, *et al.* Absence of VEGFR-1/Flt-1 signaling pathway in mice results in insensitivity to discogenic low back pain in an established disc injury mouse model. *J Cell Physiol* 2019, 235: 5305–5317
27. Chen S, Lei L, Li Z, Chen F, Huang Y, Jiang G, Guo X, *et al.* Grem1 accelerates nucleus pulposus cell apoptosis and intervertebral disc degeneration by inhibiting TGF-β-mediated Smad2/3 phosphorylation. *Exp Mol Med* 2022, 54: 518–530
28. Pfirrmann CWA, Metzdorf A, Zanetti M, Hodler J, Boos N. Magnetic resonance classification of lumbar intervertebral disc degeneration. *Spine* 2001, 26: 1873–1878
29. Ragni E, Colombini A, De Luca P, Libonati F, Viganò M, Perucca Orfei C, Zagra L, *et al.* miR-103a-3p and miR-22-5p are reliable reference genes in extracellular vesicles from cartilage, adipose tissue, and bone marrow cells. *Front Bioeng Biotechnol* 2021, 9: 632440
30. Yang D, Yuan Q, Balakrishnan A, Bantel H, Klusmann JH, Manns MP, Ott M, *et al.* MicroRNA-125b-5p mimic inhibits acute liver failure. *Nat Commun* 2016, 7: 11916
31. Yang C, Yang C, Huang Z, Zhang J, Chen N, Guo Y, Zahoor A, *et al.* Reduced expression of miR-125a-5p aggravates LPS-induced experimental acute kidney injury pathology by targeting TRAF6. *Life Sci* 2022, 288: 119657
32. Cheng X, Zhang G, Zhang L, Hu Y, Zhang K, Sun X, Zhao C, *et al.* Mesenchymal stem cells deliver exogenous miR-21 *via* exosomes to inhibit nucleus pulposus cell apoptosis and reduce intervertebral disc degeneration. *J Cell Mol Medi* 2018, 22: 261–276
33. Zhu G, Yang X, Peng C, Yu L, Hao Y. Exosomal miR-532-5p from bone marrow mesenchymal stem cells reduce intervertebral disc degeneration by targeting RASSF5. *Exp Cell Res* 2020, 393: 112109
34. He X, Zheng Y, Liu S, Shi S, Liu Y, He Y, Zhang C, *et al.* MiR-146a protects small intestine against ischemia/reperfusion injury by down-regulating TLR4/TRAF6/NF-κB pathway. *J Cell Physiol* 2018, 233: 2476–2488
35. Jiang J, Zhang J, Wu C, Chen C, Bao G, Xu G, Xue P, *et al.* Knockdown of TRAF6 inhibits chondrocytes apoptosis and inflammation by suppressing the NF-κB pathway in lumbar facet joint osteoarthritis. *Mol Cell Biochem* 2021, 476: 1929–1938
36. Zhang Y, Li S, Hong J, Yan J, Huang Z, Wu J, Deng Z, *et al.* Chromobox homolog 4 overexpression inhibits TNF-α-induced matrix catabolism and senescence by suppressing activation of NF-κB signaling pathway in nucleus pulposus cells. *Acta Biochim Biophys Sin* 2022, 7: 1021–1029
37. Hai B, Mao T, Du C, Jia F, Liu Y, Song Q, Pan X, *et al.* USP14 promotes pyroptosis of human annulus fibrosus cells derived from patients with intervertebral disc degeneration through deubiquitination of NLRP3. *Acta Biochim Biophys Sin* 2022, 11: 1720–1730
38. DiStefano TJ, Vaso K, Danias G, Chionuma HN, Weiser JR, Iatridis JC. Extracellular vesicles as an emerging treatment option for intervertebral disc degeneration: therapeutic potential, translational pathways, and regulatory considerations. *Adv Healthcare Mater* 2022, 11: 2100596
39. Dowdell J, Erwin M, Choma T, Vaccaro A, Iatridis J, Cho SK. Intervertebral disk degeneration and repair. *Neurosurgery* 2017, 80: S46–S54

40. Zhang W, Sun T, Li Y, Yang M, Zhao Y, Liu J, Li Z. Application of stem cells in the repair of intervertebral disc degeneration. *Stem Cell Res Ther* 2022, 13: 70
41. Haufe SMW, Mork AR. Intradiscal injection of hematopoietic stem cells in an attempt to rejuvenate the intervertebral discs. *Stem Cells Dev* 2006, 15: 136–137
42. Meisel HJ, Ganey T, Hutton WC, Libera J, Minkus Y, Alasevic O. Clinical experience in cell-based therapeutics: intervention and outcome. *Eur Spine J* 2006, 15: 397–405
43. Meisel HJ, Siodla V, Ganey T, Minkus Y, Hutton WC, Alasevic OJ. Clinical experience in cell-based therapeutics: disc chondrocyte transplantation. *Biomol Eng* 2007, 24: 5–21